coatings

MDPI

Article

Improved Corrosion Resistance of 5XXX Aluminum Alloy by Homogenization Heat Treatment

In-Kyu Choi, Soo-Ho Cho †, Sung-Joon Kim †, Yoo-Shin Jo † and Sang-Ho Kim *

Department of Energy, Materials and Chemical Engineering, Korea University of Technology and Education, Cheonan-si 31253, Korea; chgg99@koreatech.ac.kr (I.-K.C.); zosuho@koreatech.ac.kr (S.-H.C.); eriokim@koreatech.ac.kr (S.-J.K.); joyooshin@koreatech.ac.kr (Y.-S.J.)

* Correspondence: shkim@koreatech.ac.kr; Tel.: +82-41-560-1325

† These authors contributed equally to this work.

Received: 30 November 2017; Accepted: 15 January 2018; Published: 18 January 2018

Abstract: The corrosion resistance of homogenized Al-Mg (6.5%) alloy—adding Si, Zn, Mn, and Fe (0.2%) to improve various properties—was observed. Differential scanning calorimetry (DSC) and a JMatPro simulation revealed that the optimal homogenization temperature was 450 °C. The homogenization was carried out at 450 °C for 3, 6, 12, 18, 24, and 30 h in order to view the corrosion resistance change. Corrosion resistance was analyzed by a polarization test in 3.5 wt % NaCl solution. The corrosion resistance improved with increasing homogenization time up to 24 h, but there was no change with longer time periods. To observe the reason for the change in corrosion resistance, scanning electron microscopy coupled with energy dispersive X-ray spectroscopy (SEM-EDS), X-ray diffraction (XRD), and transmission electron microscopy coupled with energy dispersive X-ray spectroscopy (TEM-EDS) analyses were performed. Precipitates containing Mg, such as Al_3Mg_2 and $Mg_{32}(Al, Zn)_{49}$, decreased at the grain boundary. After homogenization, the amount of Mg measured by SEM-EDS at the grain boundary decreased from 36% to 8%, while Si increased. Generally, the potential difference between the grain boundary and the grains leads to intergranular corrosion. Reduction of Mg, whose standard electrode potential is lower than that of Al, and an increase of Si, which is present in higher concentration than Al at the grain boundaries, improved the corrosion resistance of 5XXX Al alloy by reducing the intergranular corrosion.

Keywords: aluminum alloy; corrosion resistance; homogenization; polarization test

1. Introduction

As the automotive industry has gradually become more sophisticated and subdivided, fuel economy regulations are becoming more stringent to address environmental issues. Accordingly, fuel efficiency improvement technology has been attracting a great deal of attention [1,2]. Among ways to improve fuel efficiency, adopting lighter weight vehicles is thought to be the most promising approach because it is expected to greatly improve the fuel efficiency through changes of structure, replacement of heavy materials with lightweight materials and reduction of the number of parts. Currently, non-ferrous metals such as Al and Mg are the mainly used light metals [3]. Among them, Al is 33% lighter than Fe, has higher strength and is excellent in terms of machining, thermoelectric conductivity, and low temperature brittleness [4]. Among the Al alloys, the Al 5000 series is an alloy containing Mg added to conventional Al. Mg has a high solubility limit in the Al matrix and a strong solid solution strengthening effect. At the same time, it has excellent ductility [5,6]. Also, Al 5000 alloys are generally used as an extruded material, but they contain Fe and Si and can also be used as casting materials. Alloys that can be used for both casting and extrusion improve the recyclability. However, when 3% or more of magnesium is added, β(Al_3Mg_2) phase, precipitated continuously at the grain boundaries, undergoes stress corrosion cracking and intergranular corrosion [7–9]. To solve this

problem, Zn is added to the Al 5000 series alloy. This leads to precipitation of $\tau(Mg_{32}(Al, Zn)_{49})$ phases and prevention of β phases at the grain boundaries, thereby improving the corrosion resistance and enhancing the mechanical properties [10]. In addition, alloy elements can be added to fulfill various goals. For example, Si improves the fluidity for casting [11]. Mn improves the tensile strength without decreasing the corrosion resistance. Fe prevents adhesion of liquid Al to the mold [12,13]. With these many aims, a new complex-composition Al alloy was investigated. Homogenization of the Al alloy distributes the secondary phase and thereby improves the tensile properties [14] and corrosion resistance [15]. However, research into the effect of homogenization on the corrosion behavior of Al-Mg-Zn alloys with Si, Fe, and Mn elements has not been reported. Therefore, in this study, the corrosion resistance of a new Al alloy was investigated depending on the homogenization time.

2. Experimental Details

The chemical composition of the Al 5XXX alloy is shown in Table 1. Specimens were prepared by wire cutting as 10 × 10 × 20 mm^3 plates. In order to determine the optimum homogenization temperature, DSC analysis and JMatPro simulation were performed. The DSC analysis, performed by increasing the temperature by 1 °C/min up to 500 °C, recorded a change of enthalpy. Homogenization was carried out using a furnace by heating up to 450 °C at a rate of 100 °C/h and maintaining the temperature at 450 °C for 3, 6, 12, 18, 24, and 30 h; samples were then air cooled. For the polarization test, the surface of the specimen was polished with #2000 emery paper and washed with distilled water; this was followed by drying using nitrogen gas.

Table 1. Chemical composition of the Al 5XXX alloy (all in wt %).

Mg	Zn	Si	Mn	Fe	Cu	Ti	B	Al
6.5	1.5	0.2	0.2	0.2	0.1	0.1	0.1	Balanced

The polarization test conditions are shown in Table 2. Saturated calomel and graphite were used for the standard and counter electrodes, respectively. The electrolytic solution was water containing 3.5% NaCl. The experiment was carried out from −1.3 V to −0.2 V at a 0.5 mV/s scanning speed. Various methods were used to identify the cause of the corrosion resistance change after homogenization. An optical microscope was employed to observe the microstructure. The etching solution was Keller reagent (2 mL HF, 3 mL HCl, 5 mL HNO_3 and 190 mL water), which is mainly used for Al-Mg-Zn [16]. The volume fraction of the grain boundaries was calculated using software from MEDIA cybernetics, Image pro 5.0. XRD was utilized to observe the secondary phase change. SEM-EDS and TEM-EDS were used to analyze the secondary phase present at the grain boundaries. The specimen for TEM was a 10 um thick foil prepared using FIB. The change in Mg content at the grain boundaries was investigated using TEM-EDS line scanning.

Table 2. Polarization test conditions.

Parameter	Vaule
Start Potential (V)	−1.3
Final Potential (V)	−0.2
Scanning Speed (mV/s)	0.5
Time (s)	2200
Temperature (°C)	25
Standard Electrode	Saturated calomel electrode
Counter Electrode	Graphite electrode
Electrolyte	3.5 wt % NaCl
Specimen Density	2.6 g/cm^3

3. Results and Discussion

Figure 1 shows the results of the DSC analysis before homogenization. Power compensated DSC measures the energy required to maintain the temperature difference between the sample and the reference. Therefore, the peak at around 472.8 °C indicates heat flow compensating for the endothermic reaction. Since the melting point of Al is higher than 600 °C, this peak does not mean Al melting; rather, it indicates the dissolution of a secondary phase. The homogenization temperature was hence decided to set at below 470 °C [17].

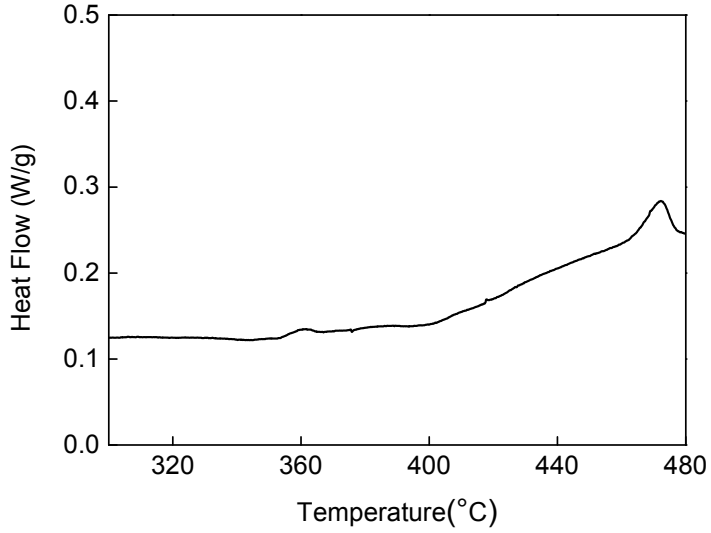

Figure 1. DSC analysis before homogenization.

Figure 2 shows the JMatPro simulation results illustrating the secondary phase formation with temperature change. The possible precipitates in Al 5XXX alloys are β(Al_3Mg_2), τ(Mg_{32}(Al, Zn)$_{49}$), Al_6(Mn, Fe), AlMgCuZn, and Mg_2Si. The dissolution at 478.2 °C, shown in Figure 1, corresponds to β and/or τ phase. Since the dissolution temperature of the β phase in the ordinary Al-Mg alloy is near 470 °C, the effective homogenization temperature for the β, τ phase reduction without Mg_2Si dissolution was considered to be 450 °C.

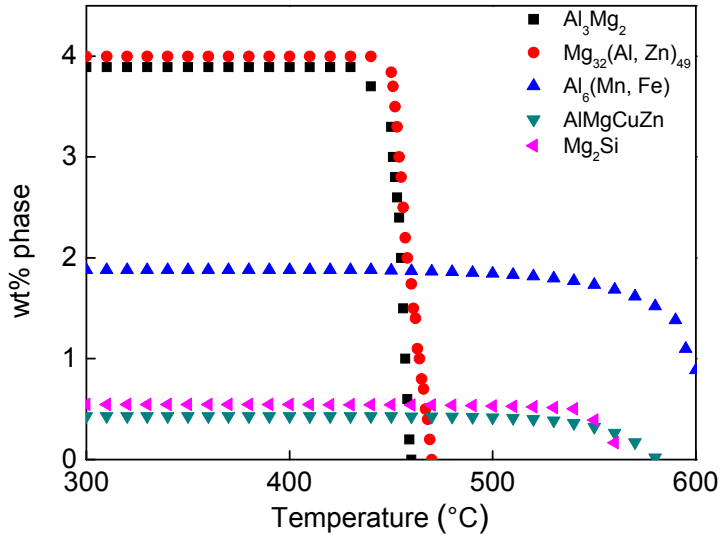

Figure 2. JMatPro simulation analyzing the second phase formation.

Figure 3 illustrates the results of the polarization test. Tafel test was carried out to determine the change of potential and current density with homogenization time. In Figure 3a, the potential can be seen not to change with increasing homogenization time. This is because there was no significant change in the alloy composition with homogenization. The corrosion rate expressed in Equations (1) and (2) in ASTM G102 can be calculated from the measured current density in the Tafel test [18].

$$\text{Corrosion rate (mmpy)} = \frac{3.27 \times 10^{-3} \times i_{\text{corr}} \times E{\cdot}W}{\text{density}\left(\frac{\text{g}}{\text{cm}^3}\right)} \quad (1)$$

$$E{\cdot}W = \frac{1}{\sum \frac{n_i f_i}{W_i}} \quad (2)$$

where i_{corr}, current density [$\mu A/cm^2$]; mmpy, mm/year (in corrosion depth); f_i, the mass fraction of the i^{th} element in the alloy; W_i, the atomic weight of the element; n_i, the number of electrons required to oxidize an atom of the element in the corrosion process, i.e., the valence of the element.

When the homogenization was carried out at 450 °C for up to 24 h, the corrosion rate decreased steadily and it was saturated after 24 h. The optimum homogenization time for improving the corrosion resistance was thus determined to be 24 h.

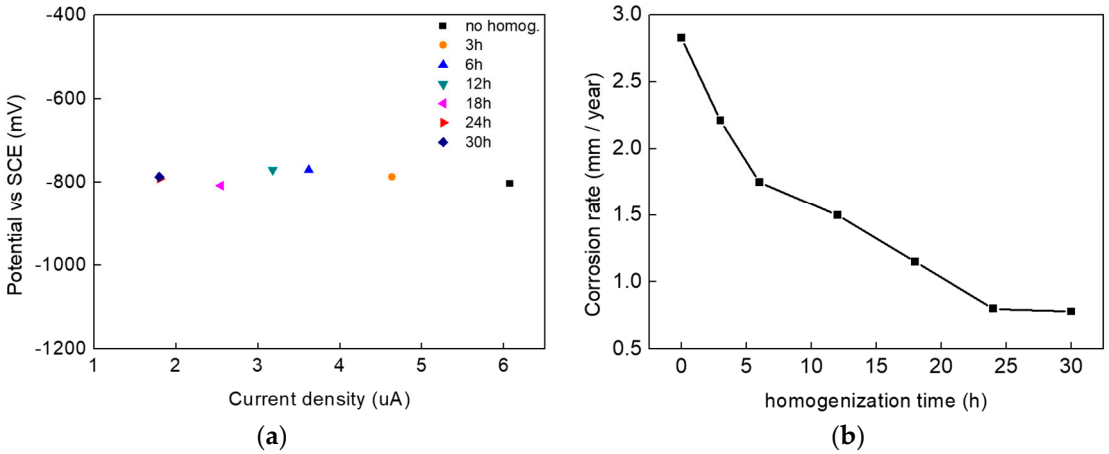

Figure 3. (**a**) Polarization potential obtained from Tafel analysis; (**b**) Corrosion rate calculated from the polarization current density of Tafel analysis.

Figure 4 demonstrates the change in microstructure with homogenization time. In order to numerically express the grain boundary volume fraction, program calculation was carried out and the results are shown in Figure 4h. Due to the grain growth, the grain boundary volume fraction decreases as the homogenization time increases to 24 h. After 24 h, the decrease slows, as anticipated by Fick's law; a similar result was reported by Li et al. [19]. The shapes in Figures 3b and 4h were very similar. Therefore, it can be considered that the corrosion rate and grain boundary are closely correlated.

Figure 5 displays X-ray diffraction analysis results confirming the existence of a secondary phase during the homogenization. Before the homogenization, peaks (8 8 0) and (10 6 2), which can be indexed to the β phase, and peak (6 3 1), which is ascribed to the τ phase [20], are observed. After 24 h of homogenization, the β and τ phases disappeared due to the dissolution of the second phases.

Figure 6 and Table 3 show the SEM-EDS analysis results of the secondary phase before homogenization. In Figures 2 and 6 and Table 3, we observed β(Al_3Mg_2), τ(Mg_{32}(Al, Zn)$_{49}$), Mg_2Si and Al_6(Mn, Fe). Phase A is considered to be a mixture of β and τ phases with a small amount of Cu. Phases B and D, frequently observed around phase A, are similar to Al_6(Mn, Fe). Phase C is Mg_2Si.

Figure 7 and Table 4 present SEM-EDS images and the composition of the secondary phases at the grain boundary after homogenization. The main secondary phase in the grain boundaries was

likely Si and/or Mg_2Si, as can be identified in Table 4. This means that $\beta(Al_3Mg_2)$, $\tau(Mg_{32}(Al, Zn)_{49})$ phases are reduced during homogenization at the grain boundaries and Si and/or Mg_2Si are formed. The difference in the composition of Si and Mg_2Si between 24 h and 30 h was not clear.

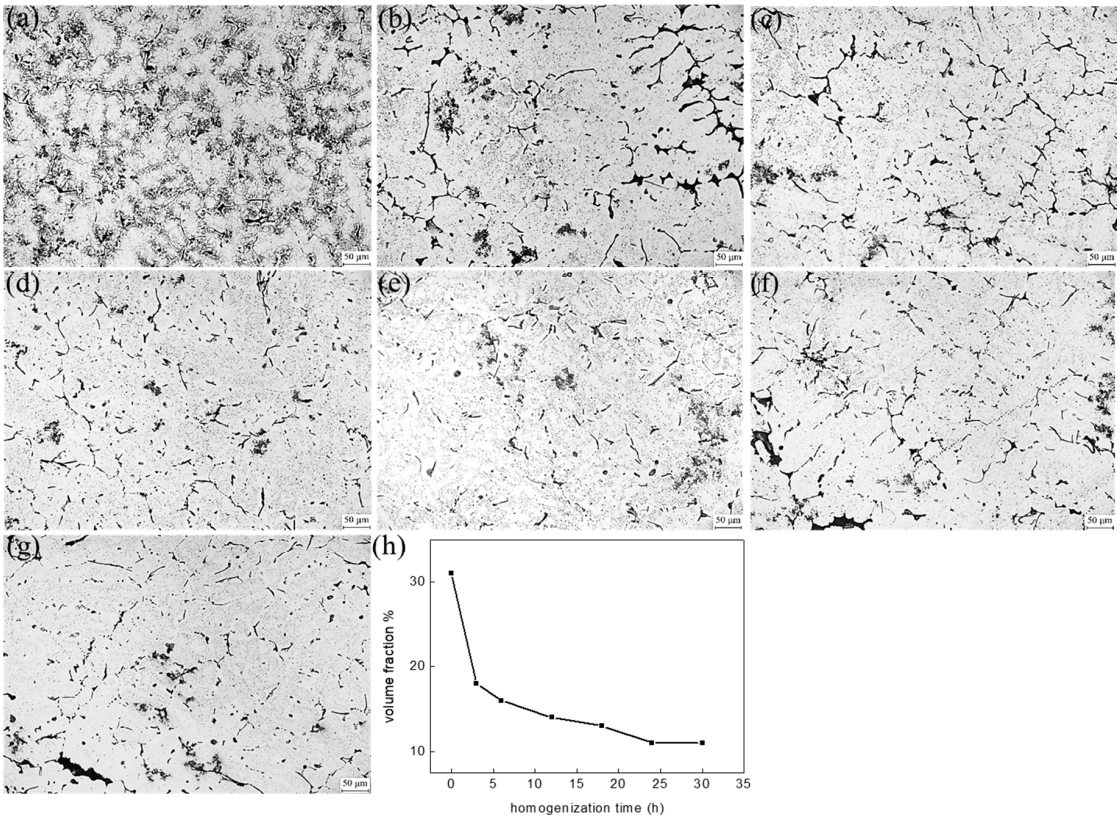

Figure 4. Optical microstructure depending on the homogenization time (×100): (**a**) no homogenization, (**b**) 3 h, (**c**) 6 h, (**d**) 12 h, (**e**) 18 h, (**f**) 24 h, and (**g**) 30 h at 450 °C; (**h**) volume fraction of grain boundary calculated by Image pro 5.0.

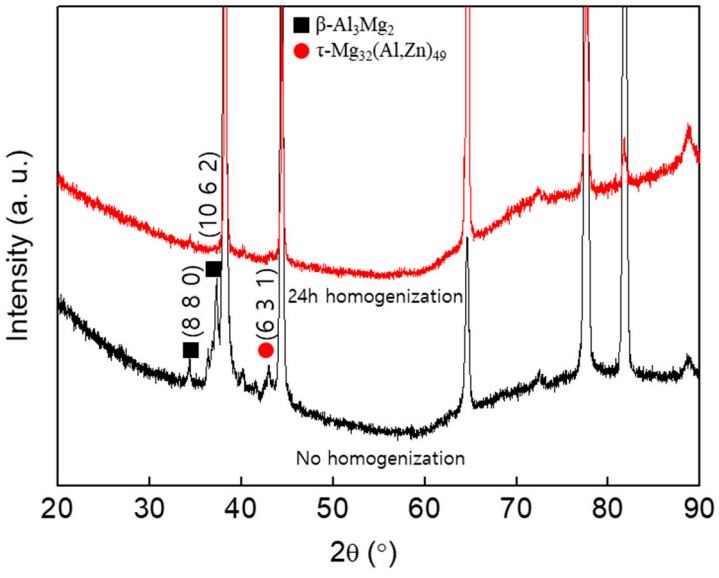

Figure 5. XRD analyses with no and 24 h homogenization.

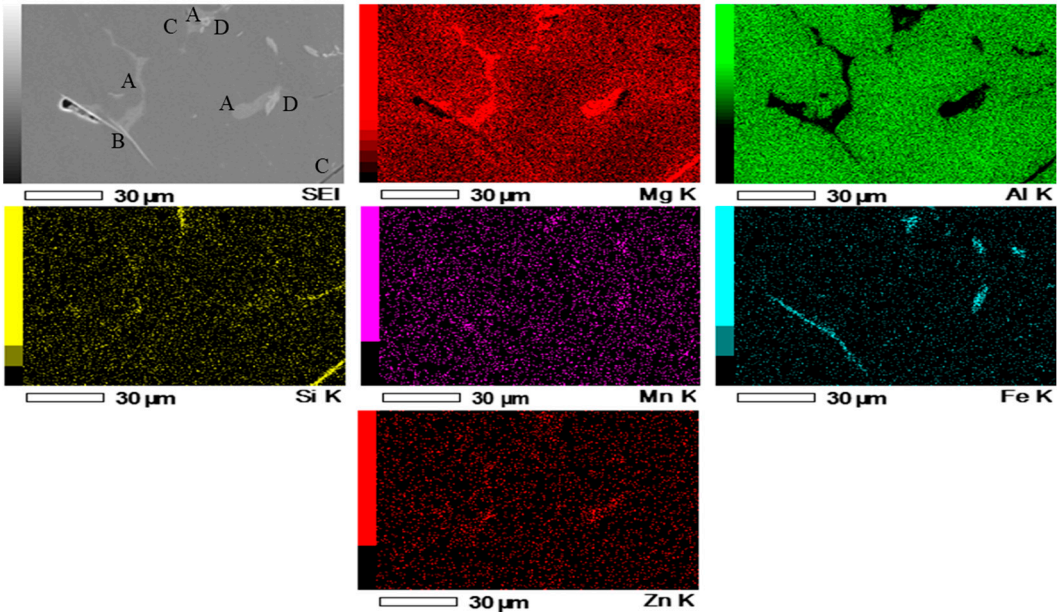

Figure 6. SEM-EDS mapping of secondary phases before homogenization.

Table 3. Chemical composition of secondary phases in Figure 6 before homogenization.

Phase	Composition (wt %)						
	Al	Mg	Zn	Fe	Mn	Si	Cu
A	51.54	37.64	7.73	–	–	–	3.09
B	79.81	8.82	–	4.34	7.03	–	–
C	87.67	8.37	–	–	–	3.96	–
D	69.73	10.66	–	2.43	17.18	–	–

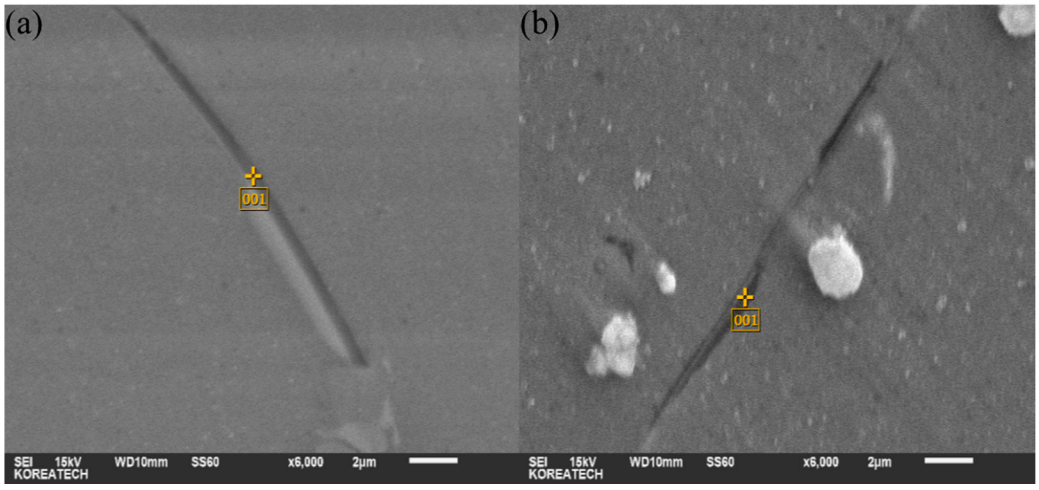

Figure 7. SEM-EDS secondary phase analysis after homogenization at: (**a**) 450 °C, 24 h; (**b**) 450 °C, 30 h.

Table 4. Chemical composition of secondary phases in Figure 7 after homogenization.

Phase	Composition (wt %)						
	Al	Mg	Zn	Fe	Mn	Si	Cu
(a)	90.39	8.22	–	–	–	1.39	–
(b)	90.60	8.06	–	–	–	1.34	–

Figure 8 displays the SEM-EDS composition map after 24 h homogenization. The map confirms again that secondary phases such as β and τ almost completely disappear at the grain boundary and, instead, levels of Mg_2Si and Si increased after homogenization. This can be explained by diffusion, following the Arrhenius equation below

$$D = D_0 \exp\left[-\frac{Q}{RT}\right] \quad (3)$$

where D_0, diffusion coefficient [m^2/s]; R, mole gas constant; Q, diffusion activation energy [kJ/mole]; T, thermodynamic temperature.

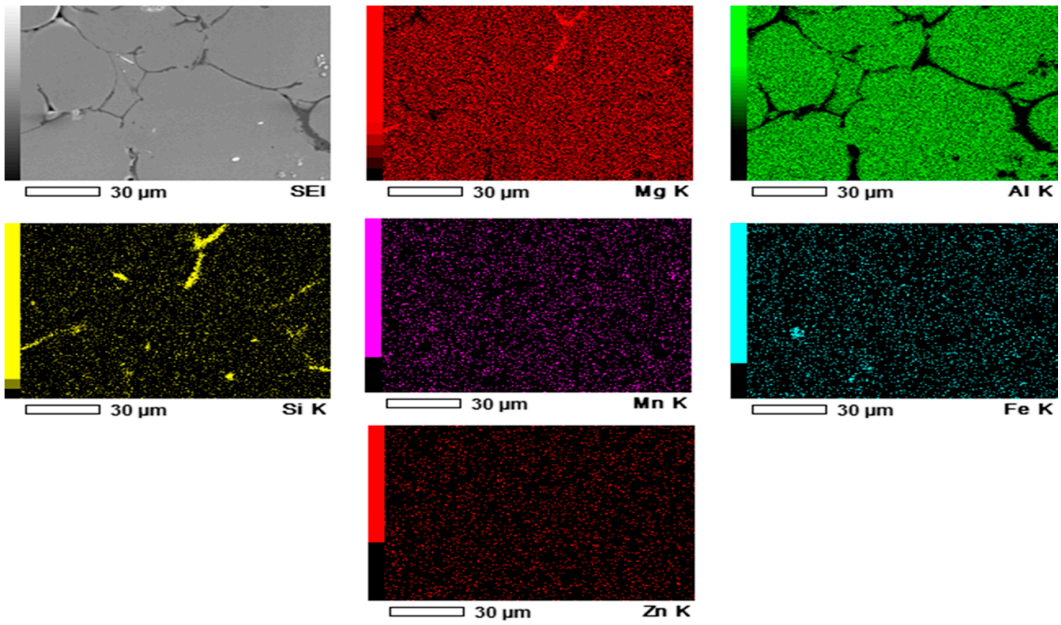

Figure 8. SEM-EDS mapping of secondary phases after homogenization.

In Equation (3), the diffusion activation energy Q of Si is larger than those of Mg, Mn, and Fe [21]. Accordingly, the distribution of Si at the grain boundaries increases with temperature. The presence of Si at the grain boundary at high temperature prevents the precipitation of other phases and increases the potential of the grain boundary via the high potential of Si after homogenization [22]. This potential increase can decelerate the intergranular corrosion. In addition, the β phase is known to form easily at grain boundaries as well as at the periphery of Al_6(Mn, Fe) [23]. The reduction of the Al_6(Mn, Fe) phase at the grain boundary by homogenization can decrease the precipitation of β phases at the grain boundary because β phases prefer to precipitate around Al_6(Mn, Fe).

As shown before in Figures 6 and 8, amounts of Mg, Mn, Fe, and Zn decrease with homogenization. This means β, τ, Al_6(Mn, Fe) phases decrease. On the contrary, Si increases by homogenization at the grain boundary. The corrosion of β and τ, which mainly contain Mg, activate galvanic corrosion because the standard reduction potential of Mg is lower than that of Al [24,25]. As reported by Zeng et al., in the Al6000 alloy, Mg accelerated inter-granular corrosion with a standard reduction potential, which is lower than that of Al; Si has with a higher standard reduction potential than discontinuous Mg_2Si, which acts as a sacrificial anode to improve corrosion resistance, especially at the grain boundary [26]. Similarly, for the Al 5XXX alloy in this study, Mg containing β and τ phases in the grain boundary significantly lowers the grain boundary potential, but Si, with higher potential and sacrificial Mg_2Si, can increase the grain boundary potential. A decrease in Mg and increases in Si and Mg_2Si at the grain boundary by homogenization, therefore, would be the main reason for the improvement of the corrosion resistance.

Figure 9 shows results of TEM-EDS line scanning of the interface between the Al matrix and the secondary phase after homogenization for 24 h at 450 °C. After the homogenization, a remainder of Mg_2Si phase was confirmed.

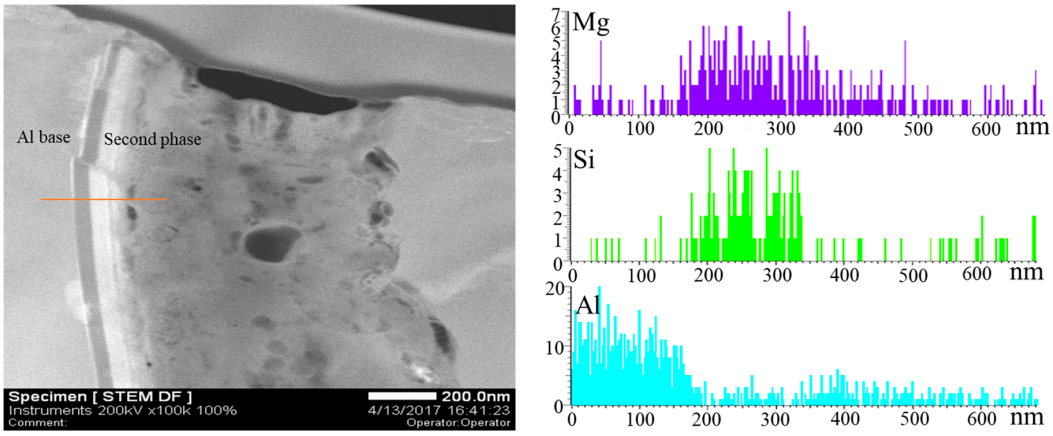

Figure 9. (**a**) TEM image; (**b**) TEM-EDS line scanning profile of the interface between Al matrix and second phase after 24 h homogenization at 450 °C.

4. Conclusions

In this study, a new Al-Mg-Zn-Mn-Fe-Si Al 5XXX alloy was homogenized and the corrosion resistance was investigated. Homogenization was conducted at 450 °C for 3, 6, 12, 18, 24, and 30 h.

The corrosion resistance improved steadily with homogenization time and saturated after 24 h. With homogenization, the grain boundary volume fraction decreased and the corrosion rate decreased. The second phases recognized at the grain boundary are mainly $\beta(Al_3Mg_2)$, $\tau(Mg_{32}(Al, Zn)_{49})$, and $Al_6(Mn, Fe)$ before homogenization and Mg_2Si and Si after homogenization.

The secondary phase present in the grain boundary had a large amount of Mg before homogenization and it is thought that the Mg, with a lower standard reduction potential, would intensify the intergranular corrosion.

With homogenization, the β and τ phase with high Mg content decreased at the grain boundary by diffusion into grains, while Si preferentially diffused to the grain boundary at high temperature homogenization can remain in Si and/or Mg_2Si at the grain boundary. Furthermore, the high reduction potential of Si and sacrificial Mg_2Si would reduce the intergranular corrosion, resulting in the better corrosion resistance of the newly developed Al 5XXX alloy.

Acknowledgments: This work was financially supported by the Korea University of Technology and Education.

Author Contributions: Sang-Ho Kim and In-Kyu Choi conceived and designed the experiments; In-Kyu Choi performed the experiments; In-Kyu Choi, Soo-Ho Cho, Sung-Joon Kim, and Yoo-Shin Jo analyzed the data; In-Kyu Choi, Soo-Ho Cho, Sung-Joon Kim, and Yoo-Shin Jo contributed reagents/materials/analysis tools; Sang-Ho Kim and In-Kyu Choi wrote the paper.

Conflicts of Interest: The authors declare no conflict of interest. The founding sponsors had no role in the design of the study; in the collection, analyses, or interpretation of data; in the writing of the manuscript, or in the decision to publish the results.

References

1. Adam, H. Carbon fiber in automotive applications. *Mater. Des.* **1997**, *18*, 349–355. [CrossRef]
2. Erica, R.-F.; Frank, R.-F.; Richard, R.; Randolph, E.-K. Strategic materials selection in the automobile body: Economic opportunities for polymer composite design. *Compos. Sci. Technol.* **2008**, *68*, 1989–2002.
3. Jürgen, H. Aluminum in innovative light-weight car design. *Mater. Trans.* **2011**, *52*, 818–824.

4. Miller, W.-S.; Zhuang, L.; Bottema, J.; Wittebrood, A.-J.; Smet, P.-D.; Haszler, A.; Vieregge, A. Recent development in aluminum alloys for the automotive industry. *Mater. Sci. Eng.* **2000**, *280*, 37–49. [CrossRef]
5. Jones, R.-H.; Baer, D.-R.; Danielson, M.-J.; Vetrano, J.-S. Role of Mg in the stress corrosion cracking of an Al-Mg alloy. *Metall. Mater. Trans. A* **2001**, *32*, 1699–1711. [CrossRef]
6. Kim, J.-M.; Seong, K.-D.; Jun, J.H.; Kim, K.-T.; Jung, W.-J. Variation of fluidity and mechanical properties of Al-Mg alloys with the addition of Si, Mn and Zn. *J. Korean Foundry Soc.* **2004**, *24*, 138–144.
7. Searles, J.-L.; Gouma, P.-I.; Buchheit, R.-G. Stress corrosion cracking of sensitized AA5083. *Metall. Mater. Trans. A* **2001**, *32*, 2859–2867. [CrossRef]
8. Romhanji, E.; Popović, M.; Glišić, D.; Stefanović, M.; Milovanović, M. On the Al-Mg Alloy sheets for automotive application: Problems and solutions. *Metalurgija* **2004**, *10*, 205–216.
9. Braun, R. Environmentally assisted cracking of aluminum alloys in chloride solutions. In Proceedings of the ICAA-6: 6th International Conference on Aluminium Alloys, Toyohashi, Japan, 5–10 July 1998; pp. 153–164.
10. Meng, C.; Zhang, D.; Hua, C.; Zhuang, L.; Zhang, J. Mechanical properties, intergranular corrosion behavior and microstructure of Zn modified Al–Mg alloys. *J. Alloy. Compd.* **2014**, *617*, 925–932. [CrossRef]
11. Cho, J.-I.; Kim, C.-W. Effects of Mg and Si on microstructure and mechanical properties of Al-Mg die casting alloy. *J. Korean Foundry Soc.* **2012**, *32*, 219–224. [CrossRef]
12. Davis, J.-R. Fabrication and Finishing of Aluminum Alloys. In *Aluminum and Aluminum Alloys*; Davis, J.-R., Ed.; ASM International: Novelty, OH, USA, 1991; pp. 351–416.
13. Yun, H.-S.; Kim, J.-M.; Park, J.-S.; Kim, K.-T. Properties and casting characteristics of Al-Zn-Fe-Si alloys. *J. Korean Foundry Soc.* **2013**, *33*, 8–12. [CrossRef]
14. Park, J.-H.; Lee, D.-H.; Nam, S.-W. Effect of Mn addition and homogenization heat treatment on the tensile properties in Al-Mg-Si alloy system. *J. Korean Inst. Met. Mater.* **1997**, *35*, 281–287.
15. Popović, M.; Romhanji, E. Stress corrosion cracking susceptibility of Al–Mg alloy sheet with high Mg content. *J. Mater. Proc. Technol.* **2002**, *125*, 275–280. [CrossRef]
16. Cerri, E.; Evangelista, E. Metallography of Aluminum alloys. In *TALAT Lecture 1202: Metallography of Aluminum Alloys*; Core-Materials: Liverpool, UK, 2009; pp. 1–20.
17. Jiang, H.-C.; Ye, L.-Y.; Zhang, X.-M.; Gu, G.; Zhang, P.; Wu, Y.-L. Intermetallic phase evolution of 5059 aluminum alloy during homogenization. *Trans. Nonferrous Met. Soc. China* **2013**, *23*, 3553–3560. [CrossRef]
18. *ASTM G102 Standard Practice for Calculation of Corrosion Rates and Related Information from Electrochemical Measurements*; ASTM: West Conshohocken, PA, USA, 1994; pp. 416–422.
19. Li, H.-Y.; Su, X.-J.; Yin, H.; Huang, D.-S. Microstructural evolution during homogenization of Al-Cu-Li-Mn-Zr-Ti alloy. *Nonferrous Met. Soc. China* **2013**, *23*, 2543–2550. [CrossRef]
20. Auld, J.-H.; Williams, B.-E. X-ray powder data of Tphases composed of aluminium and magnesium with silver, copper or zinc. *Acta Cryst.* **1966**, *21*, 830–831. [CrossRef]
21. Du, Y.; Chang, Y.-A.; Huang, B.; Gong, W.; Jin, Z.; Xu, H.; Yuan, Z.; Liu, Y.; He, Y.; Xie, F.-Y. Diffusion coefficients of some solutes in fcc and liquid Al: Critical evaluation and correlation. *Mater. Sci. Eng. A* **2003**, *363*, 140–151. [CrossRef]
22. Tan, L.; Allen, T.-R. Effect of thermomechanical treatment on the corrosion of AA5083. *Corros. Sci.* **2010**, *52*, 548–554. [CrossRef]
23. Yan, J.; Andrea, M.-H. Study of β precipitation and layer structure formation in Al 5083: The role of dispersoids and grain boundaries. *J. Alloy. Compd.* **2017**, *703*, 242–250. [CrossRef]
24. Sukiman, N.-L.; Gupta, R.-K.; Buchheit, R.-G.; Birbilis, N. Influence of microalloying additions on Al-Mg alloy. Part 1: Corrosion and electrochemical response. *Corros. Eng. Sci. Technol.* **2014**, *49*, 254–262. [CrossRef]
25. Jones, D.-A. *Principles and Prevention of Corrosion*; Macmillan Publishing Co.: London, UK, 1992.
26. Zeng, F.-L.; Wei, Z.-L.; Li, J.-F.; Li, C.-X.; Tan, X.; Zhang, Z.; Zheng, Z.-Q. Corrosion mechanism associated with Mg_2Si and Si particles in Al−Mg−Si alloys. *Trans. Nonferrous Met. Soc. China* **2011**, *21*, 2559–2567. [CrossRef]